





Article

Ce:Nd:YAG Solar Laser with 4.5% Solar-to-Laser Conversion Efficiency

Dário Garcia , Dawei Liang * , Cláudia R. Vistas, Hugo Costa, Miguel Catela , Bruno D. Tibúrcio 
and Joana Almeida

Centre of Physics and Technological Research, Departamento de Física, Faculdade de Ciências e Tecnologia, Universidade NOVA de Lisboa, 2829-516 Caparica, Portugal; kongming.dario@gmail.com (D.G.); c.vistas@fct.unl.pt (C.R.V.); hf.costa@campus.fct.unl.pt (H.C.); m.catela@campus.fct.unl.pt (M.C.); brunotiburcio78@gmail.com (B.D.T.); jla@fct.unl.pt (J.A.)

* Correspondence: dl@fct.unl.pt

Abstract: The efficiency potential of a small-size solar-pumped laser is studied here. The solar laser head was composed of a fused silica aspheric lens and a conical pump cavity, which coupled and redistributed the concentrated solar radiation from the focal zone of a parabolic mirror with an effective collection area of 0.293 m² to end-side pump a Ce (0.1 at%):Nd (1.1 at%):YAG rod of 2.5 mm diameter and 25 mm length. Optimum solar laser design parameters were found through Zemax[®] non-sequential ray-tracing and LASCAD[™] analysis. The utilization of the Ce:Nd:YAG medium with small diameter pumped by a small-scale solar concentrator was essential to significantly enhance the end-side pump solar laser efficiency and thermal performance. For 249 W incoming solar power at an irradiance of 850 W/m², 11.2 W multimode solar laser power was measured, corresponding to the record solar-to-laser power conversion efficiency of 4.50%, being, to the best of our knowledge, 1.22 times higher than the previous record. Moreover, the highest solar laser collection efficiency of 38.22 W/m² and slope efficiency of 6.8% were obtained, which are 1.18 and 1.02 times, respectively, higher than the previous records. The lowest threshold solar power of a Ce:Nd:YAG solar-pumped laser is also reported here.

Keywords: solar-pumped laser; Ce:Nd:YAG; parabolic mirror; laser efficiency



Citation: Garcia, D.; Liang, D.; Vistas, C.R.; Costa, H.; Catela, M.; Tibúrcio, B.D.; Almeida, J. Ce:Nd:YAG Solar Laser with 4.5% Solar-to-Laser Conversion Efficiency. *Energies* **2022**, *15*, 5292. <https://doi.org/10.3390/en15145292>

Academic Editor: Tapas Mallick

Received: 29 June 2022

Accepted: 19 July 2022

Published: 21 July 2022

Publisher's Note: MDPI stays neutral with regard to jurisdictional claims in published maps and institutional affiliations.



Copyright: © 2022 by the authors. Licensee MDPI, Basel, Switzerland. This article is an open access article distributed under the terms and conditions of the Creative Commons Attribution (CC BY) license (<https://creativecommons.org/licenses/by/4.0/>).

1. Introduction

Solar-pumped lasers can directly convert the incoherent broadband radiation into coherent narrowband radiation through an active medium, while the conventional lasers utilize the electric-to-light conversion from diodes or lamps. The direct harnessing of solar energy is a promising renewable technology that may bring important economic advantages for countries with high solar availability [1], for the development of sustainable industry [2], on earth [3,4] or in space [5].

In 1963, a calcium fluoride crystal doped with divalent dysprosium (Dy²⁺:CaF₂) was used to generate the first continuous-wave laser emission of 2.36 μm, by Kiss et al. [6]. From then on, several attempts to increase the solar laser efficiency have been made using different gain medium, such as gas [7,8], liquids [9], and solids [10,11]. However, only solid active media was promising enough for solar laser emission, especially the yttrium aluminum garnet (Y₃Al₅O₁₂, YAG) as hosting crystal structure and the rare earth ion of neodymium (Nd³⁺) as an activator ion, contributing to the significant advances in solar laser efficiency. About 18.7 W/m² solar laser collection efficiency, defined as laser output power versus solar collector area, was reported in 2007 by pumping a large Cr:Nd:YAG ceramic laser rod with a 1.4 m² Fresnel lens primary concentrator [12]. 19.3 W/m² laser collection efficiency was later achieved in 2011 by exciting a 4 mm diameter, 25 mm length Nd:YAG single-crystal rod through a 0.64 m² area Fresnel lens [13]. In 2012, the Nd:YAG solar laser collection efficiency was boosted to 30.0 W/m² by pumping a 6 mm diameter, 100 mm

length Nd:YAG single-crystal rod through a 4.0 m² area Fresnel lens [14]. According to the study of Zhao et al. [15], the Nd³⁺ ion absorption bands have about a 16% overlap with the solar spectrum. The solar laser output can be enhanced by adding sensitizer elements, such as chromium (Cr³⁺) or cerium (Ce³⁺) ions, which have broader absorptions bands in the visible region, increasing the energy conversion efficiency [16,17]. Although both Cr³⁺ and Ce³⁺ ions have different emission bands than that of the Nd³⁺ ion, they overlap perfectly to some of the Nd³⁺ absorption bands. Solar-pumped lasers with a Cr:Nd:YAG ceramic rod have been carried out since 2007, first by Yabe et al. [12] and later by Liang et al. in 2013 [18] and 2018 [19], but the results were not very significant, being only slightly higher than that with the Nd:YAG medium [20]. Initial stages of solar-pumping the Ce:Nd:YAG medium were conducted in the early 2020s [20], with a 5 mm diameter, 30 mm length Ce (0.05 at%): Nd (1.0 at%): YAG rod. It was end-side pumped by 960 W of incoming solar power, provided by a medium size solar furnace (MSSF) with 1.23 m² effective collection area in PROMES-CNRS [21]. In these conditions, 6.0 W laser output power was obtained. However, when increasing the incoming solar power, the rod got fractured in the upper-end region. A side-pumping scheme, which helps to spread the solar pumping radiation along the laser rod, was then adopted and tested at the NOVA heliostat-parabolic mirror system [22]. A successful solar laser emission of 16.5 W was achieved under an incoming solar power of 600 W with a Ce (0.1 at%):Nd (1.1 at%):YAG laser rod. This laser had 23.6 W/m² collection efficiency and 2.8% solar-to-laser conversion efficiency, with the latter being 1.57 times higher than that of a Nd (1.0 at%):YAG laser rod under the same conditions [22].

In 2022, Vistas et al. further explored the influence of the solar pumping distribution on a 4 mm diameter, 35 mm length Ce (0.1 at%):Nd (1.1 at%):YAG laser rod by testing two different secondary concentrators [23]: a point-focusing fused silica aspheric lens and a fused silica light guide that provided a homogenous light distribution at its output. With collection area of 1.09 m² from the MSSF parabolic mirror, the solar pumping scheme with the aspheric lens produced up to 19.6 W solar laser power before the fracture of the rod due to high thermal load, while the light guide scheme maintained continuous lasing operation, producing 17.4 W solar laser power at an incoming solar power of 1154 W. This resulted in 18 W/m² solar laser collection efficiency and 1.7% solar-to-laser conversion efficiency. The Ce:Nd:YAG solar laser initiated at an incoming solar power of 578 W, leading to 3.0% slope efficiency [23]. In the same year, Almeida et al. [24] explored the laser power scaling potential of side-pumped Ce:Nd:YAG with light guide using 2.48 m² effective collection area of the MSSF parabolic mirror [24]. 40 W solar laser output was achieved without fracturing the crystal. However, the collection, conversion, and slope efficiencies were reduced to 16.13 W/m², 1.54%, and 2.44% slope efficiencies, respectively, and the threshold power increased to 943 W. This demonstrates that the efficiency of solar laser output tends to be lower with larger collection area.

Due to the above mentioned reasons, the solar pumping of a thin Ce:Nd:YAG rod through a primary concentrator with a small effective collection area was explored here. A fused silica aspheric lens was used as a secondary concentrator for end-side-pumping the 2.5 mm diameter, 25 mm length Ce (0.1 at%):Nd (1.1 at%):YAG rod through the NOVA parabolic mirror with 0.293 m² effective collection area. During the experiments, 850 W/m² solar irradiance was measured, leading to an incoming solar power of 249.05 W. This constituted a substantial reduction from the 600 W incoming power of the most efficient Ce:Nd:YAG solar laser [22] at the same solar facility. Moreover, solar laser emission was possible, unlike the previous end-side-pumping [20] and side-pumping [23] Ce:Nd:YAG solar lasers in which the rod was fractured due to high concentrated local heat load. This resulted in 11.2 W solar laser power, corresponding to a solar laser collection efficiency of 38.22 W/m² and slope efficiency of 6.8%, which are 1.18 and 1.02 times higher than the previous state-of-the-art record [19]. More importantly, 4.50% solar-to-laser power conversion efficiency was achieved, also representing an enhancement of 1.22 times [19]. Moreover, only 88 W incoming solar power was required for Ce (0.1 at%): Nd(1.1 at%):YAG

to start lasing, as compared to the minimum of 200 W for Nd:YAG [25]. Moreover, the substantial reduction of the collection area from 1.03 m² [25] to 0.293 m² may motivate the research of small size solar laser models in direct solar tracking mode with promising possibility of further solar laser efficiency enhancement.

2. Materials and Method

2.1. Solar Energy Collection and Concentration: NOVA Heliostat-Parabolic System

The NOVA heliostat-parabolic mirror solar laser system, as shown in Figure 1, is composed of a two-axis heliostat with four flat mirrors of 93.5% reflectivity, which are used for redirecting the incoming solar radiation toward a parabolic mirror of 80.0% reflectivity with a focal length of 660 mm. This whole system has a combined reflective capacity of 74.8%. By using an external annular mask, the collection diameter of the parabolic mirror was reduced from 1.50 m to 0.68 m. About 0.293 m² effective solar collection area was then calculated by discounting the shadowed area of approximately 0.07 m² caused by the laser head and its supporting mechanics, the X-Y-Z positioner, and the non-reflecting space between the two flat segments of the heliostat.

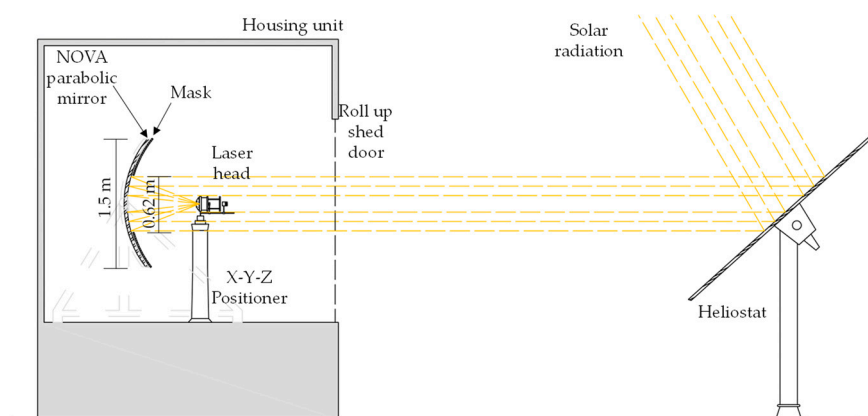


Figure 1. Schematic of the NOVA heliostat-parabolic mirror solar energy collection and concentration system.

2.2. Solar Laser Head

Figure 2 shows the image of the solar laser head and its optical components, as well as the laser resonator components. The laser head was composed of a large fused silica aspheric lens of 99.995% optical purity that focused the concentrated solar radiation onto the flat upper surface of the Ce (0.1 at%):Nd (1.1 at%):YAG rod of 2.5 mm diameter and 25 mm length, mounted within a single reflective conical pump cavity. The rod's flat upper surface had a highly reflective (HR) coating for the laser emission wavelength at 1064 nm (99.9% @ 1064 nm), while the other end surface had an anti-reflection (AR) coating for the laser emission wavelength (reflectivity (R) < 0.2% @ 1064 nm), supplied by Chengdu, Dongjun Laser Co., Ltd. (Chengdu, China). Cooling water constantly flowed into the laser head from an inlet and the heated water was extracted through the outlet. Maximum lasing could only be achieved when the laser head was correctly aligned at the focus of solar concentrator through the X-Y-Z positioner and the correct alignment of the laser resonator mirrors.

The fused silica aspheric lens had an 82 mm diameter and a thickness of 37 mm, with a curved input surface and a flat output surface. The curved feature of the aspheric lens follows the sag (z) in Equation (1), with radial aperture (r) of 41 mm, the parabolic constant $k = 0$, the radius of curvature (c) of -43 mm, and the aspheric coefficient $\beta_1 = -0.004$.

$$z = \frac{c \times r^2}{1 + \sqrt{1 - (1 + k)c^2 r^2}} + \beta_1 r^2, \quad (1)$$

The flat output surface of the lens was 6 mm apart from the flat input surface of the crystal rod. This space was necessary for the laser rod to effectively absorb the concentrated solar radiation and to guarantee an abundant cooling for effective heat dissipation. The absorption efficiency was further enhanced by a silver-coated aluminum foil of 94% reflectivity that covered the conical pump cavity. The reflective conical surface allowed the reabsorption of the solar energy due to the crisscross of the solar rays into the laser rod, thus helping in the redistribution of the solar energy along the rod. This conical pump cavity was 19.5 mm in length with input and output aperture diameters of 18 mm and 9 mm, respectively.

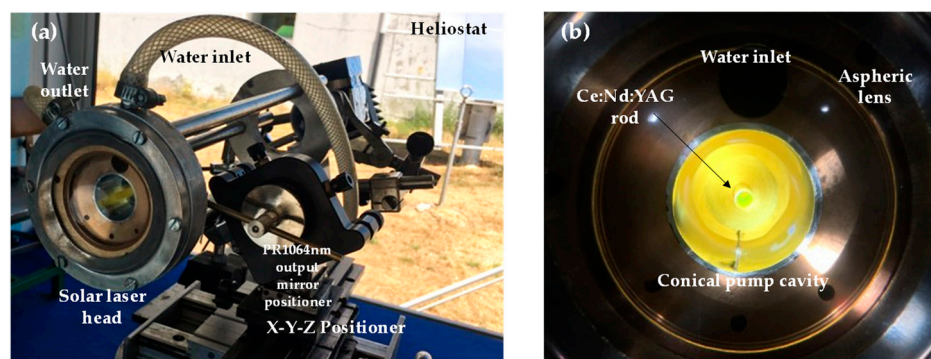


Figure 2. Photograph of (a) the Ce (0.1 at%):Nd (1.1 at%):YAG solar laser head at the focus of the parabolic mirror, and (b) the front view of the laser head.

Cooling water with 6 L/min flow rate was used as the heat extraction medium. The cooling system was designed to maximize the removal of the heat generated within the rod and the optical components, such as the fused silica aspheric lens and the conical pump cavity. Both the cooling water and the silica lens weaken the intensity of the UV solarization and IR heating arriving at the rod, which help to reduce the thermal lensing issue.

3. Theory

Energy Transfer Mechanism between Ce³⁺ and Nd³⁺ Ions in YAG

The study of Ce³⁺ ion doped in Nd:YAG under broadband pumping has been a topic of research for decades, starting in 1969 by Holloway et al. [26]. In 1987, Mares et al. studied the energy transfer mechanism between Ce³⁺ and Nd³⁺ in YAG at low temperatures [27]. Later in 2015, Tai et al. explored the mechanism of energy transfer of Ce³⁺ to Nd³⁺ in YAG with quantum cutting [28]. Its recent use in 2021 by Vistas et al., as a substitute of Nd:YAG in solar-pumped lasers, has shown promising results, achieving about 1.6 times more collection efficiency and solar-to-laser power conversion efficiency compared to that with Nd:YAG crystal rod under the same conditions [22].

The direct solar spectrum, the Ce:Nd:YAG absorption spectrum, the Ce³⁺ and Nd³⁺ ions' emission bands in YAG are presented in Figure 3. The broad absorption bands of the Ce³⁺ ion is located at the most energetic region of the electromagnetic spectrum, between 315 nm and 510 nm, corresponding to the excited energy level of 5d₂ (centered at 339 nm) and 5d₁ (centered at 460 nm) [28]. While the Nd³⁺ absorption bands are in between 510 nm and 888 nm, with five prominent absorbing bands, ⁴G_{7/2} + ²G_{9/2} + ²K_{13/2} (centered at 530 nm), ²G_{7/2} + ⁴G_{5/2} (centered at 580 nm), ⁴S_{3/2} + ⁴F_{7/2} (centered at 770 nm), ²H_{9/2} + ⁴F_{5/2} (centered at 805 nm), and ⁴F_{3/2} (centered at 878 nm) [29].

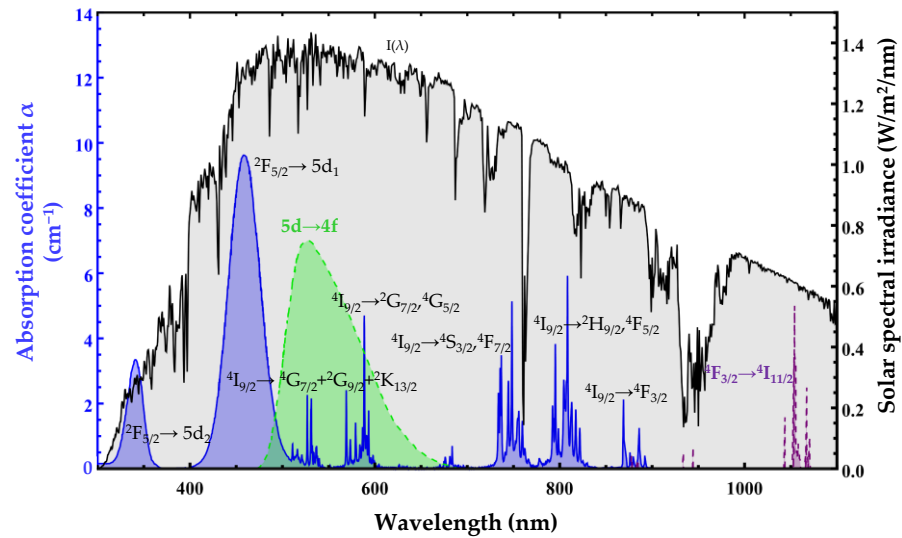


Figure 3. AM1.5 direct solar spectrum (black), adapted from [30]. Ce (0.1 at%):Nd (1.1 at%):YAG absorption spectrum (blue), Ce³⁺ (green) and Nd³⁺ (purple) emission spectra in YAG, adapted from [31].

The strong UV and blue photons excite the Ce³⁺ 4f level (the ²F_{5/2} ground state), toward the 5d sublevels of 5d₁ and 5d₂, as shown in Figure 4 [28,32]. The consequent energy relaxation from 5d₁ to both ground states ²F_{7/2} and ²F_{5/2} forms a yellow/green broad emission spectrum, overlapping with the excitation peaks of the Nd³⁺ ion at the ⁴G_{7/2} + ²G_{9/2} + ²K_{13/2} energy levels between 510 nm and 540 nm and the ²G_{7/2} + ⁴G_{5/2} energies levels between 566 nm and 595 nm [28,33]. The radiative transfer mechanism by the transition 5d → 4f of the Ce³⁺ ion and the transitions ⁴I_{9/2} → ⁴G_{7/2} + ²G_{9/2} + ²K_{13/2} and ⁴I_{9/2} → ²G_{7/2} + ⁴G_{5/2} through cross-relaxation process are indicated by pathway (1) in Figure 4 [28]. The pathway (2) represents the energy transfer from the Ce³⁺ excited state at 5d₁ to the two Nd³⁺ ions at ⁴F_{3/2} level through quantum cutting down-conversion process [28].

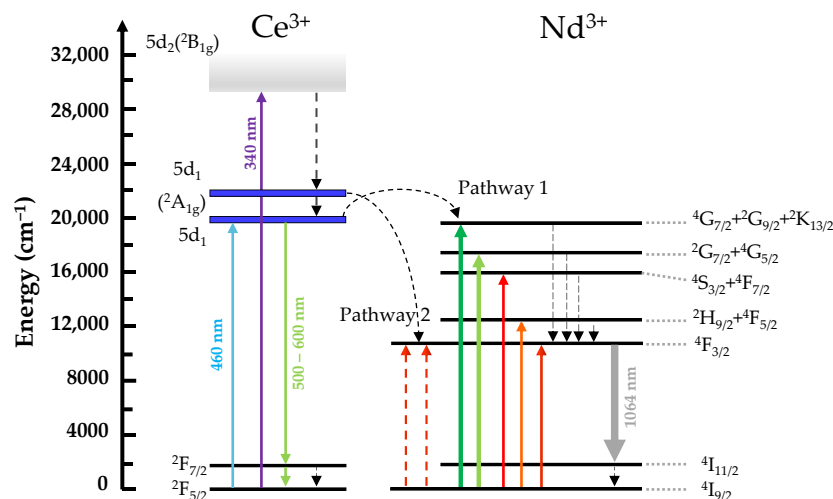


Figure 4. Absorption and emission energy level of Ce³⁺ and Nd³⁺ ions. (1) The energy transfer by cross relaxation of Ce³⁺ to Nd³⁺ ion, and (2) the quantum cutting down conversion of Ce³⁺ ion from 5d₁ energy level into two Nd³⁺ ions at ⁴F_{3/2} energy level. Adapted from [28,29].

The total absorbed solar power of an ion ($P_{abs,ion}$) of the active medium is calculated through Equation (2).

$$P_{abs,ion} = \int_{\lambda_i}^{\lambda_f} I(\lambda) \left(1 - e^{(-\alpha_{ion}(\lambda) \times L_c)}\right) d\lambda, \quad (2)$$

$I(\lambda)$ is the solar spectral irradiance ($W/m^2/nm$) of each wavelength λ , L_c is the effective absorption length of the laser rod and $\alpha_{ion}(\lambda)$ is the absorption coefficient of the ion for each wavelength. To effectively calculate the total power available from the Sun to feed both ions, L_c must be considered infinite. In this case, the total absorbed power by Ce^{3+} ($P_{abs,Ce}$) and Nd^{3+} ($P_{abs,Nd}$) ions is approximately 157 W and 162 W, respectively. Given the total solar irradiance of $1000 W/m^2$, by integrating all the solar wavelength intensities, the overlap efficiency, i.e., the fraction of the available solar power that is absorbed by the Ce^{3+} ($\eta_{overlap,Ce}$) and Nd^{3+} ($\eta_{overlap,Nd}$) ions, is about 15.7% and 16.2%, respectively, as calculated through Equation (3).

$$\eta_{overlap,ion} = \frac{P_{abs,ion}}{\int I(\lambda) d\lambda} \quad (3)$$

The energy transfer efficiency of the non-radiative process ($\eta_{NR,Ce-Nd}$) is about 70% [28,34], whereas for the radiative process ($\eta_{R,Ce-Nd}$) is about 30% [28].

4. Calculation

4.1. Zemax[®] Simulation

There are many possible and viable ways to calculate the absorbed power within the Ce:Nd:YAG with the prevalent wavelengths in the Zemax[®] software. A direct approach for calculation consists of using all the wavelengths of both the solar emission and the Ce:Nd:YAG absorption spectra. However, this method would require much more computing resources to achieve the same results as those by simulating with a few key solar wavelengths related to the absorption bands responsible for lasing [35].

A total available solar power of 249.05 W can be obtained by the NOVA parabolic mirror with an effective collection area (A) of $0.293 m^2$, at $850 W/m^2$ solar irradiance (I). However, only 16.2% and 15.7% of the total power calculated from Equation (3) are useful for calculating the absorbed power by the Ce:Nd:YAG rod with finite dimensions. Consequently, in Zemax[®], two sources were defined for solar pumping. The energy division is shown in Figure 5a.

Source 1 emits all the relevant overlapped wavelengths of the solar spectrum with the Nd^{3+} ion absorption spectrum, as well as the wavelength data that includes the Ce^{3+} quantum cutting down conversion of non-radiative transfer to Nd^{3+} , described by Pathway (1), as shown in Figure 5b. The simulated power of source 1 ($P_{source1}$) follows the Equation (4) and has a total power of 67.72 W.

$$P_{source1} = A I \left(\eta_{overlap,Nd^{3+}} + \eta_{overlap,Ce^{3+}} \times \eta_{NR,Ce-Nd} \right), \quad (4)$$

Source 2 accounts for 30% of the absorbed energy by Ce^{3+} that was transferred radiatively to Nd^{3+} , as shown in Figure 4 by Pathway (2). This source emits green and orange wavelengths useful for Nd^{3+} absorption, as shown in Figure 5c. The simulated power of source 2 ($P_{source2}$) follows the Equation (5) and has a total power of 11.73 W.

$$P_{source2} = A I \eta_{overlap,Ce^{3+}} \times \eta_{R,Ce-Nd}, \quad (5)$$

The amount of energy retained within the Ce (0.1 at%):Nd (1.1 at%):YAG depends on the transmission (T) data of the Nd^{3+} active ion, water and silica materials, shown in Equation (6).

$$T(\lambda) = e^{-\alpha(\lambda) \times L_c}, \quad (6)$$

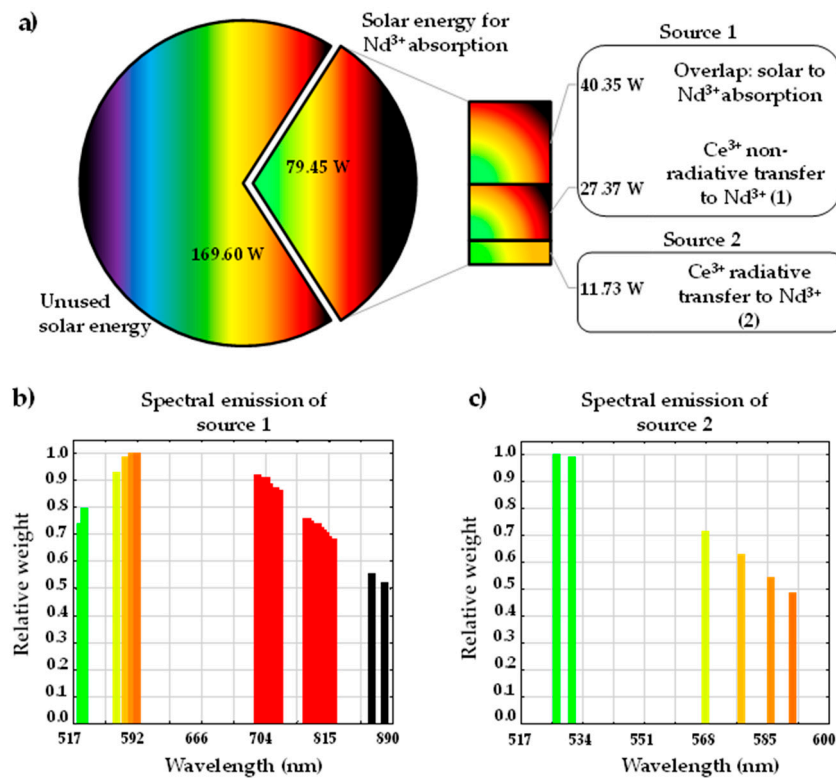


Figure 5. (a) Solar energy division for Ce:Nd:YAG absorption from a total of 249.05 W. Spectral composition used in (b) source 1 and (c) source 2.

Figure 6a shows the transmission data of water and fused silica materials from Zemax[®] glass catalog, as well as the 22 transmission wavelengths of Ce (0.1 at%):Nd (1.1 at%):YAG, at $L_c = 10$ mm. Figure 6b shows the index of refraction of Ce (0.1 at%):Nd (1.1 at%):YAG, water and fused silica as a function of the wavelength utilized in Zemax[®].

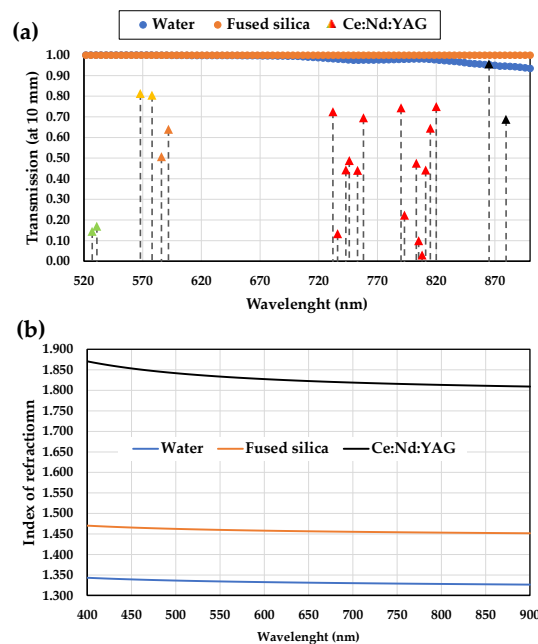


Figure 6. Materials in Zemax[®]: Ce (0.1 at%):Nd (0.1 at%):YAG, water and fused silica. (a) Transmission of the materials at 10 mm depth. (b) Index of refraction of the materials at 20 °C and 1 atm.

The transmission and the refractive index of the optical materials, the shape of each optical apparatus, the solar wavelengths and the angle of the concentrated solar rays determine the optical path of the solar rays from the source to the crystal rod. Figure 7 shows the optical path of the concentrated solar rays arriving at the laser head, through the fused silica aspheric lens, then into the cooling water and finally to the Ce:Nd:YAG crystal rod. Most of the concentrated solar rays enter the laser rod through its upper HR1064 nm end face, and travel within the rod through total internal reflection (due to the refractive index differences between the water and the active medium), as shown in Figure 7 by the red ray. Side-pumping occurs when rays enter the rod through its lateral surface. Multiple passes can be achieved by a single ray zigzagging back into the crystal through the conical pump cavity, which increases the path length of the ray inside the rod, L_p , and hence the amount of energy absorbed.

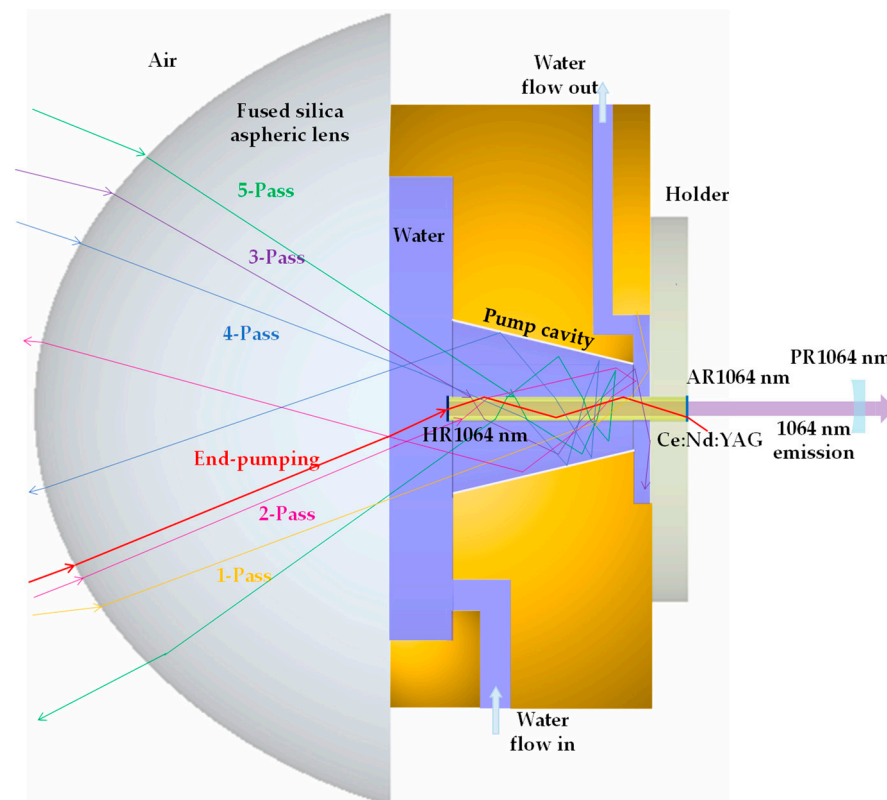


Figure 7. Solar rays at various angles and wavelengths passing through the Ce:Nd:YAG medium inside the laser head. End-pumping occurs through total internal reflection within the rod. Side-pumping may have 1 to 5 or more passes through the rod.

Figure 8 shows the absorption of the laser rod as a function of the wavelength and the number of passes. The end-pump has a minimum L_p of 25 mm, the same as the length of the rod. The average L_p of 1-pass, 2-pass, 3-pass, 4-pass, and end-pumping is about 3.25 mm, 6.50 mm, 9.75 mm, 13 mm, and 35 mm, respectively. The absorption of a single ray increases gradually with each successive number of passes within the crystal. Some wavelengths, such as 527 nm, 531 nm, 736 nm, 793 nm, 805 nm, and 808 nm are totally absorbed by the rod if the ray is traveling within the rod by end-pumping regime.

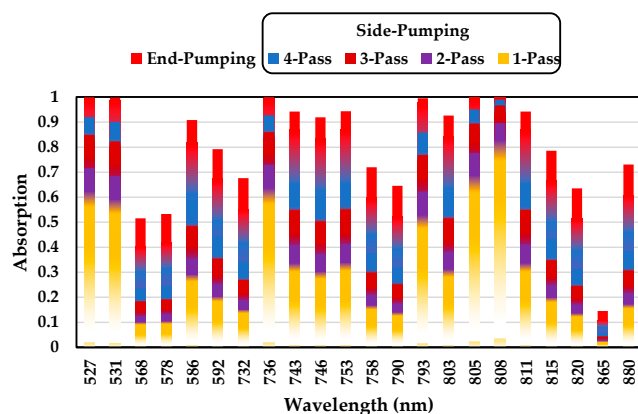


Figure 8. Wavelength-dependent absorption versus number of passes within the crystal. Each pass covers an average absorption length traveled within the crystal rod.

In Zemax[®], the Ce (0.1 at%):Nd (1.1 at%):YAG rod was divided into 125,000 voxels. The pump flux distribution along its longitudinal cross-section and five central transversal cross-sections are shown in Figure 9. Red color represents the maximum solar energy absorption, whereas blue represents little or no absorption. The most intensive absorbing region has a peak flux of 0.95 W/mm^3 , located slightly below the input surface of the rod. The lower part of the rod also absorbs some radiation due to multiple passages of the solar rays by side-pumping with the help of the reflective cone. A total absorbed solar energy of 30.96 W was stored along the thermally loaded crystal.

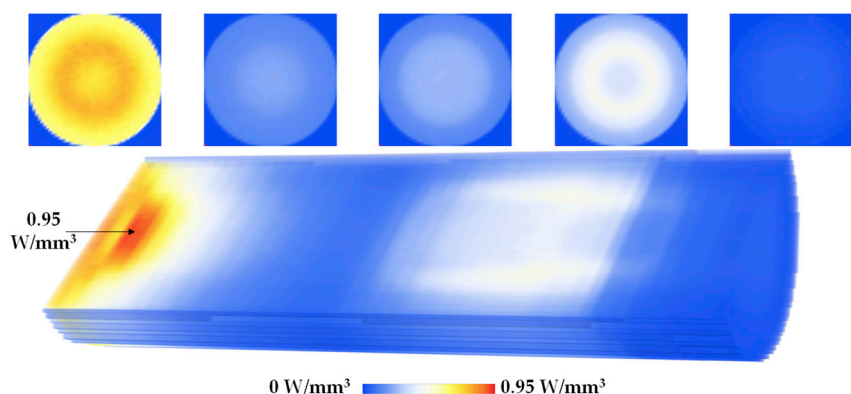


Figure 9. Absorbed solar pump-flux distribution along the longitudinal at a central cross-section, and five separate transversal cross-sections of the Ce:Nd:YAG rod.

4.2. LASCAD[™] Simulation

The absorbed power in cubic matrix form was imported into the laser cavity analysis and design (LASCAD[™]) software to analyze the solar laser output performance. The material data of Ce (0.1 at%):Nd (1.1 at%):YAG crystal with a stimulated emission cross-section of $2.8 \times 10^{-19} \text{ cm}^2$, a fluorescence lifetime of 230 μs and an absorption/scattering loss of 0.002 cm^{-1} was set in LASCAD[™]. The mean absorbed and intensity-weighted wavelength of 660 nm was considered in the analysis [11]. Figure 10 shows the laser resonator of the thermally loaded crystal rod and the associated dielectric lenses. The left end-face of the rod has a layer of HR 1064 nm coating, represented by the optical dielectric interface 0. The output end-face has an AR 1064 nm coating, represented by the optical dielectric interface 1. The partial reflection (PR) output mirror is positioned 17 mm apart from the AR coated end face ($L_{\text{AR-PR}} = 17 \text{ mm}$), represented by optical dielectric interface 2. Different reflectivities and radii of curvature (RoC) of the PR mirror were tested to find the best combination to achieve the highest laser output power for the most

efficiently solar-pumped Ce:Nd:YAG rod. A total round-trip loss of 1.6% was accounted in the LASCAD™ calculation.

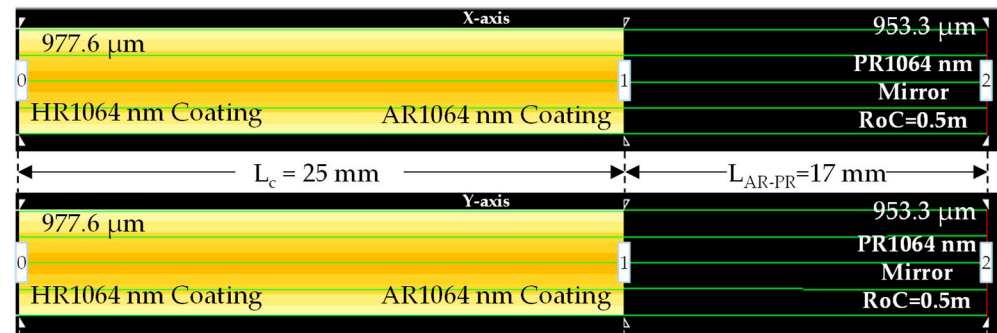


Figure 10. Laser resonator configuration for multimode solar laser extraction from the Ce:Nd:YAG rod. The L_c is the laser rod length, and the L_{AR-PR} is the length between AR1064 nm end face of the rod and the PR1064 nm mirror.

Figure 11 shows the heat load, the temperature, and the stress intensity of the 2.5 mm diameter, 25 mm length rod numerically calculated through LASCAD™ analysis, under ambient temperature and cooling boundary condition of 300 K. The maximum heat load of 0.385 W/mm^3 was locally found. A maximum rod temperature of 313.8 K is attained at the tip of the input surface of the crystal. A moderate maximum thermal stress of 24.23 N/mm^2 was found.

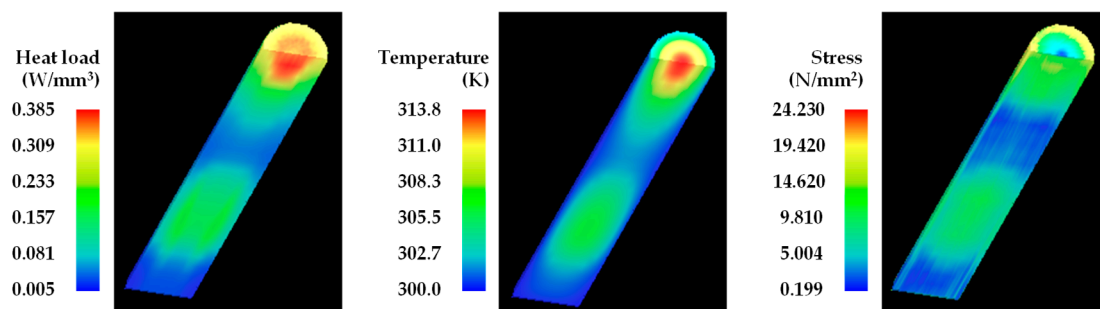


Figure 11. Heat load, temperature, and stress intensity of the 2.5 mm diameter, 25 mm length Ce:Nd:YAG rod, numerically acquired through LASCAD™ analysis.

During the solar laser experiments, the thin Ce:Nd:YAG rod was cooled by water with a constant flow rate of 6 L/min at 300 K ambient temperature. This allowed the maximum temperature within the crystal to rise no more than just 14 K with the concentrated solar pumping, as shown in Figure 11. According to [36], this temperature variation leads to a decrease in the stimulated emission cross section of only $0.05 \times 10^{-19} \text{ cm}^2$ approximately. Hence, its effect on the Nd^{3+} ions absorption bands is minimal.

Considering all the mentioned physical characteristics of the stimulated active medium, the highest multimode laser power of 11.3 W was numerically calculated with a PR1064 nm of $R = 96\%$, RoC of 0.5 m, as shown in Figure 12. The experimental results are also given.

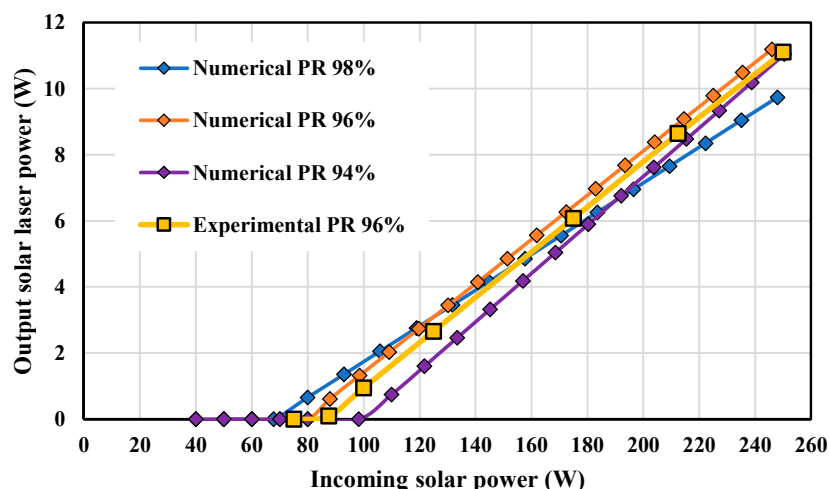


Figure 12. Ce:Nd:YAG solar laser output power as a function of the incoming solar power, numerically obtained using partial reflection (PR) mirror of 94%, 96%, and 98% and experimentally achieved with PR 96%.

5. Results and Discussion

The solar laser head prototype was built according to the model designed in Zemax[®] that provided the highest laser power extraction through LASCAD[™]. The laser head was tested at the NOVA solar facility in April of 2022. The solar irradiance of 850 W/m² was measured during that period, which is equivalent to a maximum incoming solar power of 249 W provided from the primary parabolic mirror with effective diameter of 0.68 m. A maximum multimode laser power of 11.2 W was successfully achieved using a PR (R ≥ 96% @ 1064 nm) mirror with RoC of 0.5 m, as shown in Figure 12, which matches well with the numerical prediction. The lasing emission started with an incoming solar power of 88 W and grew linearly to 11.2 W at 249 W incoming solar power, leading to a slope efficiency of 6.8%.

Table 1 summarizes the most recent progress in solar-pumped lasers, regarding to the minimum threshold power, maximum solar-to-laser power conversion, solar laser collection, and slope efficiencies.

In this work, only 88 W solar power was needed to start the lasing process, which is 0.44 times below the record minimum threshold power of 200 W [25]. The solar lasing system was able to produce 11.2 W multimode laser power, equivalent to the highest solar-to-laser power conversion efficiency of 4.50%, to the best of our knowledge, which is 1.22 times more than the record of 3.69% [19]. Furthermore, the solar laser collection and slope efficiencies were 38.22 W/m² and 6.8%, respectively, being 1.18 and 1.02 times higher than the previous records of 32.5 W/m² and 6.7% through an end-side-pumped Cr:Nd:YAG rod [19].

Table 1. Comparison of progress in solar efficiencies.

Parameters	Guan et al. 2018 [25]	Liang et al. 2018 [19]	Vistas et al. 2021 [22]	This Work 2022	Improvements Over Previous Record (Times)
Primary concentrator	Fresnel lens	Parabolic mirror	Parabolic mirror	Parabolic mirror	-
Overall efficiency of the collection system	~45%	75%	75%	75%	-
Effective collection area	1.030 m ²	1.000 m ²	1.070 m ²	0.293 m ²	-
Tracking method	Direct tracking	Via heliostat	Via heliostat	Via heliostat	-
Solar irradiance	980 W/m ²	870 W/m ²	860 W/m ²	850 W/m ²	-

Table 1. Cont.

Parameters	Guan et al. 2018 [25]	Liang et al. 2018 [19]	Vistas et al. 2021 [22]	This Work 2022	Improvements Over Previous Record (Times)
Active medium	Nd:YAG/YAG	Cr:Nd:YAG	Ce:Nd:YAG	Ce:Nd:YAG	-
Pumping method	End-side-pump	End-side-pump	Side-pump	End-side-pump	-
Laser power	31.1 W	32.5 W	16.5 W	11.2 W	-
Minimum incoming threshold power	200 W	400 W	220 W	88 W	0.44 [25]
Solar-to-laser conversion efficiency	3.1%	3.7%	2.8%	4.5%	1.22 [19]
Solar laser collection efficiency	32.1 W/m ²	32.5 W/m ²	23.6 W/m ²	38.22 W/m ²	1.18 [19]
Slope efficiency	5.4%	6.7%	4.4%	6.8%	1.02 [19]

The laser beam M^2 quality factors of the Ce:Nd:YAG were measured according to ISO 11164-1 standards, with a CINOGY UV-NIR beam profiler using a CinCam CMOS. Figure 13a shows the multimode laser beam profile. The measured solar laser beam widths along the beam caustic and the associated extrapolated hyperbolic plot are shown in Figure 13b. $M_x^2 = 32.16 \pm 2.62$ and $M_y^2 = 36.62 \pm 4.22$ factors were experimentally obtained.

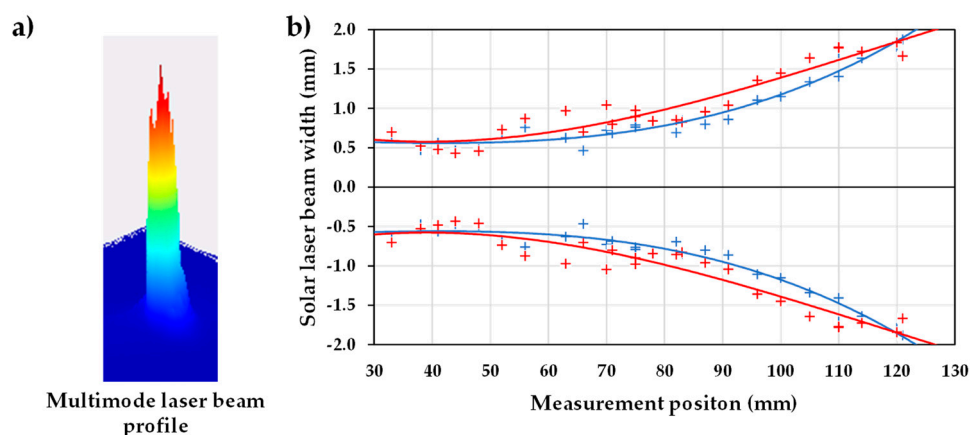


Figure 13. (a) Multimode beam profile. (b) Caustic fit measurements of the multimode solar laser beam along the X-axis (red color) and Y-axis (blue color).

6. Conclusions

The highly efficient Ce:Nd:YAG solar laser was composed of the first-stage heliostat-parabolic mirror solar energy collection and concentration system; the second-stage fused silica aspheric lens that further concentrated the solar energy onto the end-face of the active medium by end-pumping; and the third-stage conical-shaped reflective pump cavity to efficiently side-pump the 2.5 mm diameter, 25 mm length Ce:Nd:YAG rod. The solar energy transfer for the Nd³⁺ and Ce³⁺ ions as well as the energy transfer of Ce³⁺ to Nd³⁺ were introduced and considered in Zemax[®]. The design parameters of the laser head were optimized to find the highest solar energy absorption by the active medium to then determine the best lasing conditions in LASCAD[™]. The Ce:Nd:YAG solar laser prototype was then built according to the simulated model. 11.2 W multimode laser output power was successfully measured, matching well with the numerical result. This, to the best of our knowledge, resulted in a record solar-to-laser conversion efficiency of 4.50%. The highest solar laser collection and slope efficiencies of 38.22 W/m² and 6.8%, respectively, were also

obtained. Furthermore, low threshold power of 88 W was also reported. Since the NOVA solar energy collection and concentration facility has a limited transfer efficiency of 0.75, further research on small size Ce:Nd:YAG solar laser in direct solar tracking mode will, most hopefully, ensure further solar laser efficiency enhancement and enable promising space applications.

Author Contributions: Conceptualization, D.G.; methodology, D.G.; software, D.G., D.L., C.R.V., H.C. and M.C.; validation, D.G. and D.L.; formal analysis, D.G., D.L., C.R.V. and J.A.; investigation, D.G.; resources, D.L. and J.A.; data curation, D.G. and D.L.; writing—original draft preparation, D.G.; writing—review and editing, D.G., D.L., C.R.V., M.C., B.D.T., H.C. and J.A.; visualization, D.G.; supervision, D.L.; project administration, D.L.; funding acquisition, D.L. All authors have read and agreed to the published version of the manuscript.

Funding: This research was funded by Fundação para a Ciência e a Tecnologia—Ministério da Ciência, Tecnologia e Ensino Superior, grant number UIDB/00068/2020.

Institutional Review Board Statement: Not applicable.

Informed Consent Statement: Not applicable.

Data Availability Statement: Not applicable.

Acknowledgments: The contract CEECIND/03081/2017 and the fellowship grants SFRH/BD/145322/2019, PD/BD/142827/2018, PD/BD/128267/2016 and SFRH/BPD/125116/2016 of Joana Almeida, Miguel Catela, Dário Garcia, Bruno D. Tibúrcio, and Cláudia R. Vistas, respectively, are acknowledged.

Conflicts of Interest: The authors declare no conflict of interest. The funders had no role in the design of the study; in the collection, analyses, or interpretation of data; in the writing of the manuscript, or in the decision to publish the results.

Nomenclature

A	Collection area (m^2)
c	Radius of curvature (mm)
I	Solar irradiance (W/m^2)
k	Parabolic constant
$P_{abs,ion}$	Absorbed solar power by ion (W)
L_c	Length rod (mm)
L_{AR-PR}	Distance between AR and PR (mm)
r	Radial aperture (mm)
R	Reflectivity
z	Sag (mm)
Greek symbol	
α_{ion}	Absorption coefficient (cm^{-1})
β_1	Aspheric coefficient (mm^{-1})
$\eta_{overlap,ion}$	Overlap efficiency
$\eta_{NR:Ce-Nd}$	Non-radiative conversion efficiency of Ce^{3+} to Nd^{3+}
λ	Wavelength (nm)
Abbreviation	
AR	Anti-reflection
HR	High reflection
LASCAD™	Laser cavity analysis and design
MSSF	Medium sized solar furnace
PR	Partial reflection
RoC	Radius of curvature
YAG	Yttrium aluminum garnet

References

1. The Global Goals. Goal 7: Affordable and Clean Energy. Available online: <https://www.globalgoals.org/goals/7-affordable-and-clean-energy/> (accessed on 1 April 2022).
2. The Global Goals. Goal 9: Industry, Innovation and Infrastructure. Available online: <https://www.globalgoals.org/goals/9-industry-innovation-and-infrastructure/> (accessed on 1 April 2022).
3. Motohiro, T.; Takeda, Y.; Ito, H.; Hasegawa, K.; Ikesue, A.; Ichikawa, T.; Higuchi, K.; Ichiki, A.; Mizuno, S.; Ito, T.; et al. Concept of the solar-pumped laser-photovoltaics combined system and its application to laser beam power feeding to electric vehicles. *Jpn. J. Appl. Phys.* **2017**, *56*, 08MA07. [CrossRef]
4. Yabe, T.; Bagheri, B.; Ohkubo, T.; Uchida, S.; Yoshida, K.; Funatsu, T.; Oishi, T.; Daito, K.; Ishioka, M.; Yasunaga, N.; et al. 100 W-class solar pumped laser for sustainable magnesium-hydrogen energy cycle. *J. Appl. Phys.* **2008**, *104*, 083104. [CrossRef]
5. Abdel-Hadi, Y.A. Space-based solar laser system simulation to transfer power onto the earth. *NRIAG J. Astron. Geophys.* **2020**, *9*, 558–562. [CrossRef]
6. Kiss, Z.J.; Lewis, H.R.; Duncan, R.C. Sun pumped continuous optical maser. *Appl. Phys. Lett.* **1963**, *2*, 93–94. [CrossRef]
7. Insuik, R.J.; Christiansen, W.H. Blackbody-pumped CO₂ laser experiment. *AIAA J.* **1984**, *22*, 1271–1274. [CrossRef]
8. Terry, C.K.; Peterson, J.E.; Goswami, D.Y. Terrestrial solar-pumped iodine gas laser with minimum threshold concentration requirements. *J. Thermophys. Heat Transf.* **1996**, *10*, 54–59. [CrossRef]
9. Lee, J.H.; Kim, K.C.; Kim, K.H. Threshold pump power of a solar-pumped dye laser. *Appl. Phys. Lett.* **1988**, *53*, 2021–2022. [CrossRef]
10. Lando, M.; Kagan, J.; Linyekin, B.; Dobrusin, V. A solar-pumped Nd:YAG laser in the high collection efficiency regime. *Opt. Commun.* **2003**, *222*, 371–381. [CrossRef]
11. Weksler, M.; Schwartz, J. Solar-Pumped Solid-State Lasers. *IEEE J. Quantum Electron.* **1988**, *24*, 1222–1228. [CrossRef]
12. Yabe, T.; Ohkubo, T.; Uchida, S.; Yoshida, K.; Nakatsuka, M.; Funatsu, T.; Mabuti, A.; Oyama, A.; Nakagawa, K.; Oishi, T.; et al. High-efficiency and economical solar-energy-pumped laser with Fresnel lens and chromium codoped laser medium. *Appl. Phys. Lett.* **2007**, *90*, 261120. [CrossRef]
13. Liang, D.; Almeida, J. Highly efficient solar-pumped Nd:YAG laser. *Opt. Express* **2011**, *19*, 26399–26405. [CrossRef] [PubMed]
14. Dinh, T.H.; Ohkubo, T.; Yabe, T.; Kuboyama, H. 120 watt continuous wave solar-pumped laser with a liquid light-guide lens and an Nd:YAG rod. *Opt. Lett.* **2012**, *37*, 2670–2672. [CrossRef] [PubMed]
15. Zhao, B.; Zhao, C.; He, J.; Yang, S. Study of active medium for solar-pumped solid-state lasers. *Guangxue Xuebao Acta Opt. Sin.* **2007**, *27*, 1797–1801.
16. Yagi, H.; Yanagitani, T.; Yoshida, H.; Nakatsuka, M.; Ueda, K.-I. Highly Efficient Flashlamp-Pumped Cr³⁺ and Nd³⁺ Codoped Y₃Al₅O₁₂ Ceramic Laser. *Jpn. J. Appl. Phys.* **2006**, *45*, 133–135. [CrossRef]
17. Payziyev, S.; Makhmudov, K.; Abdel-Hadi, Y.A. Simulation of a new solar Ce:Nd:YAG laser system. *Optik* **2018**, *156*, 891–895. [CrossRef]
18. Liang, D.; Almeida, J.; Guillot, E. Side-pumped continuous-wave Cr:Nd:YAG ceramic solar laser. *Appl. Phys. B* **2013**, *111*, 305–311. [CrossRef]
19. Liang, D.; Vistas, C.R.; Tibúrcio, B.D.; Almeida, J. Solar-pumped Cr:Nd:YAG ceramic laser with 6.7% slope efficiency. *Sol. Energy Mater. Sol. Cells* **2018**, *185*, 75–79. [CrossRef]
20. Vistas, C.R.; Liang, D.; Garcia, D.; Almeida, J.; Tibúrcio, B.D.; Guillot, E. Ce:Nd:YAG continuous-wave solar-pumped laser. *Optik* **2020**, *207*, 163795. [CrossRef]
21. Li, Y.; Zhou, S.; Lin, H.; Hou, X.; Li, W. Intense 1064 nm emission by the efficient energy transfer from Ce³⁺ to Nd³⁺ in Ce/Nd co-doped YAG transparent ceramics. *Opt. Mater.* **2010**, *32*, 1223–1226. [CrossRef]
22. Vistas, C.R.; Liang, D.; Almeida, J.; Tibúrcio, B.D.; Garcia, D.; Catela, M.; Costa, H.; Guillot, E. Ce:Nd:YAG side-pumped solar laser. *J. Photonics Energy* **2021**, *11*, 1–9. [CrossRef]
23. Vistas, C.R.; Liang, D.; Garcia, D.; Catela, M.; Tibúrcio, B.D.; Costa, H.; Guillot, E.; Almeida, J. Uniform and Non-Uniform Pumping Effect on Ce:Nd:YAG Side-Pumped Solar Laser Output Performance. *Energies* **2022**, *15*, 3577. [CrossRef]
24. Almeida, J.; Liang, D.; Garcia, D.; Tibúrcio, B.D.; Costa, H.; Catela, M.; Guillot, E.; Vistas, C.R. 40 W Continuous Wave Ce:Nd:YAG Solar Laser through a Fused Silica Light Guide. *Energies* **2022**, *15*, 3998. [CrossRef]
25. Guan, Z.; Zhao, C.; Li, J.; He, D.; Zhang, H. 32.1 W/m² continuous wave solar-pumped laser with a bonding Nd:YAG/YAG rod and a Fresnel lens. *Opt. Laser Technol.* **2018**, *107*, 158–161. [CrossRef]
26. Holloway, W.W.; Kestigian, M. Optical Properties of Cerium-Activated Garnet Crystals. *J. Opt. Soc. Am.* **1969**, *59*, 60–63. [CrossRef]
27. Mares, J.; Jacquier, B.; Pédrini, C.; Boulon, G. Energy transfer mechanisms between Ce³⁺ and Nd³⁺ in YAG: Nd, Ce at low temperature. *Rev. Phys. Appl.* **1987**, *22*, 145–152. [CrossRef]
28. Tai, Y.; Zheng, G.; Wang, H.; Bai, J. Near-infrared quantum cutting of Ce³⁺–Nd³⁺ co-doped Y₃Al₅O₁₂ crystal for crystalline silicon solar cells. *J. Photochem. Photobiol. A Chem.* **2015**, *303–304*, 80–85. [CrossRef]
29. Powell, R.C. *Physics of Solid-State Laser Materials*; Springer: New York, NY, USA, 1998.
30. ASTM G173-03(2012); Standard Tables for Reference Solar Spectral Irradiances: Direct Normal and Hemispherical on 37° Tilted Surface. ASTM International: West Conshohocken, PA, USA, 2012.

31. Payziyev, S.; Sherniyozov, A.; Bakhramov, S.; Zikrillayev, K.; Khalikov, G.; Makhmudov, K.; Ismailov, M.; Payziyeva, D. Luminescence sensitization properties of Ce: Nd: YAG materials for solar pumped lasers. *Opt. Commun.* **2021**, *499*, 127283. [[CrossRef](#)]
32. Ueda, J.; Tanabe, S. (INVITED) Review of luminescent properties of Ce³⁺-doped garnet phosphors: New insight into the effect of crystal and electronic structure. *Opt. Mater. X* **2019**, *1*, 100018. [[CrossRef](#)]
33. Samuel, P.; Yanagitani, T.; Yagi, H.; Nakao, H.; Ueda, K.I.; Babu, S.M. Efficient energy transfer between Ce³⁺ and Nd³⁺ in cerium codoped Nd: YAG laser quality transparent ceramics. *J. Alloys Compd.* **2010**, *507*, 475–478. [[CrossRef](#)]
34. Yamaga, M.; Oda, Y.; Uno, H.; Hasegawa, K.; Ito, H.; Mizuno, S. Energy transfer from Ce to Nd in Y₃Al₅O₁₂ ceramics. *Phys. Status Solidi C* **2012**, *9*, 2300–2303. [[CrossRef](#)]
35. LAS-CAD GmbH. *LASCAD, 3.3.5 Manual*; LAS-CAD GmbH: Munchen, Germany, 2007.
36. Dong, J.; Rapaport, A.; Bass, M.; Szipocs, F.; Ueda, K.-I. Temperature-dependent stimulated emission cross section and concentration quenching in highly doped Nd³⁺: YAG crystals. *Phys. Status Solidi A* **2005**, *202*, 2565–2573. [[CrossRef](#)]